applied mechanics

Article

Ratcheting Response of Heat-Treated Notched 1045 Steel Samples Undergoing Asymmetric Uniaxial Loading Cycles

Faezeh Hatami and Ahmad Varvani-Farahani *

Department of Mechanical and Industrial, and Mechatronics Engineering, Toronto Metropolitan University, 350 Victoria Street, Toronto, ON M5B 2K3, Canada; fhatami@torontomu.ca
* Correspondence: avarvani@torontomu.ca; Tel.: +1-416-979-5000

Abstract: The present study evaluates the ratcheting response of notched cylindrical samples made of 1045 steel alloy subjected to asymmetric loading cycles using the kinematic hardening framework, coupled with Neuber's rule. Test samples with V-shaped and semi-circular edge notches were first heat-treated under different conditions, resulting in various material hardness values at the notch root region. Local ratcheting at the notch root of samples was found to be highly dependent on the notch shape and the heat treatment conditions. HT1 samples with a lower hardness of 12 RC at the notch region possessed higher values of ratcheting, while ratcheting at the notched region for HT2 samples with 40 RC dropped to half of that in HT1 samples. The higher hardness of 50 RC at the notch edge of HT3 samples promoted the initial yield strength and the yield surface through the kinematic hardening rule with a larger translation into the deviatoric stress space as compared with samples HT1 and HT2 with 12 and 40 RC, respectively. The local ratcheting strain in sample HT1, with semi-circular notches ($K_t = 1.65$) at a stress ratio (S_{max}/S_{ult}) of 0.965, remained below 1.80% during the first hundred loading cycles. The local ratcheting decreased to 1.2% for sample HT2 and further dropped to 0.9% for sample HT3. The yield surfaces were translated consistent with the magnitude and direction of the backstress increments, as the applied loading excursion exceeded the elastic limit. Through the use of the Ahmadzadeh–Varvani (A–V) hardening rule, the predicted ratcheting values at notch roots were found to be larger in magnitudes as compared with those of experimental data, while the predicted local ratcheting through the Chaboche (CH) hardening rule fell below the experimental data. Results consistently showed that as sample hardness increased, the local ratcheting at notch roots decreased.

Keywords: local ratcheting at notch root; heat treatment conditions; kinematic hardening rules; backstress increments; asymmetric loading cycles

check for updates

Citation: Hatami, F.; Varvani-Farahani, A. Ratcheting Response of Heat-Treated Notched 1045 Steel Samples Undergoing Asymmetric Uniaxial Loading Cycles. *Appl. Mech.* **2024**, *5*, 362–375. https://doi.org/10.3390/applmech5020021

Received: 17 January 2024
Revised: 21 April 2024
Accepted: 24 May 2024
Published: 27 May 2024

Copyright: © 2024 by the authors. Licensee MDPI, Basel, Switzerland. This article is an open access article distributed under the terms and conditions of the Creative Commons Attribution (CC BY) license (https://creativecommons.org/licenses/by/4.0/).

1. Introduction

Load-bearing components are susceptible to catastrophic failure in the presence of stress raisers, particularly when they are subjected to complex loading spectra. Engineering components undergoing asymmetric stress cycles beyond the elastic limit promote plastic strain accumulation, referred to as the ratcheting phenomenon. While ratcheting was promoted with mean stress, Wang and Rose [1] reported that local hysteresis loops shifted to lower stresses and that they became stabilized as loading cycles progressed. Hu et al. [2] found that as the applied strain increased, the local ratcheting and the rate of stress relaxation increased at the notch root. They reported that ratcheting and stress relaxation at notch roots closely agreed with the values predicted through the Chaboche hardening rule. Rahman and Hassan [3] assessed the ratcheting behavior of notched specimens by conducting uniaxial tests on SS304L plates with different notch sizes. They employed the hardening frameworks of Chaboche [4], Ohno–Wang [5], and AbdelKarim–Ohno [6] and demonstrated that the ratcheting values predicted by Chaboche's model closely agreed with the experimental data acquired in the vicinity of notch roots. Firat [7] measured

local strains in notched 1070 steel specimens using strain gauges positioned near the notch roots. To quantify local plastic strains during asymmetric axial–torsional loading cycles, Firat employed Neuber's rule [8] along with the Chaboche model. The predicted local ratcheting values at the notch root of 1070 steel specimens agreed with those reported in reference [9]. Liu et al. [10] conducted cyclic tests on elbow pipes made of austenitic stainless steel. They measured local strains along the perimeter of the pressurized elbows using strain gauges mounted around the diameter of the pipes. These measurements closely agreed with the local strains predicted by the Chen–Jiao–Kim (CJK) model [11]. More studies [12–16] have been conducted to evaluate local ratcheting progress at the root of circular notches in steel samples at different stress levels. Kolasangiani et al. [12] employed the Armstrong–Fredick (A–F) hardening framework [17] along with Neuber's rule to study local ratcheting and stress relaxation in the notched region. Shekarian and Varvani [13–16] coupled the Chaboche [4] and A–V [18] kinematic hardening models with the Neuber rule to assess ratcheting and stress relaxation at the roots of circular and elliptical notches in SS316 samples. Hatami and Varvani [19] evaluated the occurrence of local ratcheting at the notch root of 1045 steel samples subjected to uniaxial asymmetric loading cycles. They employed the A–V hardening framework in conjunction with the Neuber, Glinka, and Hoffman–Seeger (H–S) rules. The use of Neuber's rule along with the A–V model predicted local plastic strains at notch roots more consistent with the experimental data as compared with other counterpart models of Glinka and H–S.

The post-processing treatments of notched samples noticeably affected the local ratcheting resistance of materials under remotely asymmetric loading cycles. Weiyuan et al. [20] conducted fatigue tension–tension tests on aluminum Al-5Zn-2Mg samples post-welded by the process of MIG filler wire welding with an ER5356 welding electrode. They observed the progressive plastic strain mainly within the weld zone as loading cycles proceeded. Through the SEM investigation of the weld zone, they evidenced that at stresses greater than half of the tensile strength, local ratcheting was mainly promoted within the weld zone. The formation of slip bands within this zone was taken as the root cause of the weld joint failure. The microstructure and ratcheting behavior of laser MIG hybrid welding joints made of Al 6061 samples have been examined by Duan et al. [21]. The ratcheting strain of welded Al 6061 joints progressed as mean stress and stress amplitude increased. The uniaxial ratcheting of the base metal SS304L and the weld joint ER308L has been examined by Wang et al. [22]. The measured ratcheting of the base-metal and the weld joint was found to be noticeably different. The welded joint exhibited a relatively short hardening in the first few stress cycles, then a softening response occurred in single cycles until the failure stage, while the base metal possessed cyclic hardening over longer stress cycles before deviating to a softening response at failure. Gioielli et al. [23] studied the impact of ratcheting and fatigue on weld inspection and pipeline integrity. The local quasi-static and cyclic deformation of brazed AISI 304L/BAu-4 joints were studied by Schmiedt et al. [24] through the optical digital image correlation technique. They examined the deformation and ratcheting response of the brazed joints and reported that the drop in the virtual gauge length led to an increase in ratcheting, particularly at higher stresses in the brazed joints.

The effect of the cold expansion post-processing of notched samples prior to ratcheting tests has been studied by Chakherlou et al. [25–28]. They evidenced that a higher degree of press fitting improved materials in the vicinity of notch roots against the ratcheting phenomenon. Tripathy et al. [29] pre-strained ASTM A668 Class D steel samples at 2%, 4%, and 8% and reported a noticeable influence of mechanical pre-loading on the ratcheting of this alloy. As the magnitude of pre-straining increased from 2% to 8%, ratcheting strain dropped as high as 50%. The local ratcheting at the notch edge of Al 7075-T6 specimens was evaluated [30] through the use of the A–V and CH hardening rules in conjunction with the Neuber rule. Aluminum samples were initially press fitted with different degrees of interference fit. This study verified that as the degree of interference fit increased, local ratcheting at various distances of 1.3 and 3 mm within the edge of the notch roots dropped noticeably.

The effect of heat treatment post-processing on the ratcheting of samples made of commercial aluminum was studied by Kreethi et al. [31]. They evidenced a saturation/plateau in ratcheting results after 40 and 30 loading cycles for the annealed and normalized conditions, respectively. In a later study, Kreethi et al. [32] examined the ratcheting response of 42CrMo4 steel samples at various loading levels after annealing and normalizing heat treatment conditions. Ratcheting strain in the annealed samples ranged from 0.85% to 7.5%, but variances in normalized samples ranged from 0.14% to 0.78% for minimum to maximum stress magnitudes, respectively. Although significant ratcheting strain occurred in both normalized and hardened/tempered specimens, the severity of strain accumulation was more pronounced in normalized samples. Azadi and colleagues [33] also evaluated the influence of nano-clay addition and heat treatment on aluminum–silicon (Al-Si) samples. Through the precipitation hardening process, the second phase particles dispersed within the aluminum matrix, and Al-Si samples showed cyclic softening, promoting the ratcheting progress. The concurrent effects of heat treatment post-processing on ratcheting and fatigue in carbide-free bainite rail steel samples have been investigated by Xu et al. [34]. Because of the different heat treatment conditions, the 1380G rail steel microstructure possessed a finer lath and a more stable retained austenite than the 1280G rail steel. It resulted in a more homogeneous deformation in the 1380G rail steel than that in the 1280G rail steel, leading to 13.6% to 29.3% longer fatigue lives and 66.3% to 233.5% higher ratcheting strains for the 1380G rail steel. The influence of heat treatment post-processing on the ratcheting of notched 1045 steel samples was examined at different stress levels and ratios by Stephens and coworkers [35–37]. The notched specimens were heat treated at different temperatures and tempered to minimize the residual stresses, inducing different material hardnesses at notch roots and local ratcheting magnitudes.

The present study aims to predict local ratcheting at the notch edge of 1045 steel samples after heat treatment post-processing under different conditions. Ratcheting test data [35–37] of 1045 steel samples examined in this study consisted of samples (i) with V- and semi-circular-shaped notches, (ii) heat-treated under different conditions, and (iii) cyclically tested at different stress levels and under asymmetric loading cycles. Local ratcheting at notch roots was predicted through the A–V and CH hardening rules coupled with the Neuber rule. The heat treatment post-processing improved materials within the notch region against the ratcheting phenomenon. A higher hardness at the notched edge improved the steel samples against ratcheting progress. Through the use of the A–V and CH hardening rules, the evolution of yield surfaces beyond the elastic limit were discussed, as materials within the notch region possessed different yield strengths and hardnesses under different heat treatment post-processing conditions. The hardening frameworks were found to be consistent in ratcheting response for different notch shapes, stress levels, and heat treatment conditions.

2. Hardening Rule Frameworks

2.1. The Ahmadzadeh–Varvani Hardening Rule

Within the domain of plastic deformation, yield surfaces are translated with the backstress increments. The movement direction of yield surfaces in the stress space is governed by kinematic hardening models. The A–V nonlinear hardening model [18] governed the backstress evolution through the loading paths. The dynamic recovery part of this model involved an internal variable to control the gradual evolution of backstress with the loading process through the term $(\overline{\alpha} - \delta\overline{b})$. This term is crucial in allowing the yield surface to move in the deviatoric stress space, enabling the assessment of ratcheting progression with stress cycles. The A–V model possessed a streamlined framework, which made it more suitable for the efficient assessment of ratcheting with a smaller number of coefficients as compared with other prominent models. The general form of the A–V model is expressed as:

$$d\overline{\alpha} = Cd\overline{\varepsilon}_p - \gamma_1(\overline{\alpha} - \delta\overline{b})dp \quad (1)$$

$$d\overline{b} = \gamma_2(\overline{\alpha} - \overline{b})dp \quad (2)$$

The coefficients C, γ_1, and γ_2 are material-dependent and are thoroughly explained in [38]. Coefficients C and γ_1 are responsible for preserving the cyclic plasticity consistency condition, achieving the progressive and non-closed hysteresis loops under stress-controlled conditions. To control the size and shape of the hysteresis loops, material constants C and γ_1 are calibrated. Values of C and γ_1 are determined through the alignment of the experimentally obtained and the predicted loops in any given loading cycle. Coefficient γ_2 is determined from a set of ratcheting data plotted versus asymmetric loading cycles. As the magnitude of γ_2 increases, the predicted ratcheting curve shifts to a lower level. The optimal sets of coefficients offer a consistent agreement in the shape and size of the predicted and measured hysteresis loops. The non-zero value of coefficient δ is adapted to allow a gradual drop in backstress over the loading process and to prevent the term $(\overline{\alpha} - \delta\overline{b})$ from falling below zero. Coefficient δ is defined as $\delta = (\frac{\alpha}{k})^m$, where $k = \frac{C}{\gamma_1}$ and $0 < m < 1.0$ are material constants.

2.2. The Chaboche Hardening Rule

Based on Chaboche's hardening rule [4], the yield surface translation is defined by the summation of backstress increments. This kinematic hardening model translates the yield surfaces as backstress increments are integrated. As materials are deformed beyond their elastic limits, yield surfaces are translated into deviatoric stress space based on Chaboche's non-linear model as follows:

$$d\overline{\alpha} = \sum_{i=1}^{3} d\overline{\alpha}_i \tag{3}$$

$$d\overline{\alpha}_i = \frac{2}{3} C_i d\overline{\varepsilon}_p - \gamma_i{}' \overline{\alpha}_i dp \tag{4}$$

where backstress components for the loading excursions beyond elastic limit are expressed as follows [39]:

$$\alpha_i = \frac{2C_i}{3\gamma_i{}'} + (\alpha_{i0} - \frac{2C_i}{3\gamma_i{}'})\exp[-\gamma_i{}'(\varepsilon_p - \varepsilon_{p0})] \tag{5}$$

$$\alpha_i = -\frac{2C_i}{3\gamma_i{}'} + (\alpha_{i0} + \frac{2C_i}{3\gamma_i{}'})\exp[\gamma_i{}'(\varepsilon_p - \varepsilon_{p0})] \tag{6}$$

where ε_{i0} and ε_{p0} are the initial backstress and the initial plastic strain, respectively. Coefficients C_1 and C_3 were determined from a stabilized stress–strain hysteresis loop measured under the strain-controlled test condition [4]. The slope of the initial segment of the stabilized hysteresis curve, characterized by a high plastic modulus at the yield point, is used to determine coefficient C_1, whereas the linear component of the same curve is used to calculate coefficient C_3. Coefficient $\gamma_1{}'$ is large enough to keep the initial hardening parameter stable. Coefficients $\gamma_1{}'$ and $\gamma_3{}'$ are obtained using uniaxial ratcheting strain data. Hardening over the loading paths is stabilized by $\gamma_1{}'$, while $\gamma_3{}'$ is responsible for preserving the ratcheting strain steady rate. Coefficients C_2 and $\gamma_2{}'$ are defined through the use of a trial method to satisfy $\left(\frac{C_1}{\gamma_1'}\right) + \left(\frac{C_2}{\gamma_2'}\right) + \sigma_y = S - \frac{C_3}{2}[\Delta\varepsilon_p]$, where term $\Delta\varepsilon_p$ is the plastic strain range and S corresponds to the applied stress amplitude.

2.3. Stress and Strain at Notch Root

To predict local ratcheting using the CH and A–V hardening rules, the cyclic stress components at the notch root region are determined. Neuber's rule [8] was used along the hardening framework to predict the local stress during each stress cycle at a given constant strain. The applied cyclic stress and strain are related to the local stress and strain values at the notch root during the unloading and reloading paths of each cycle as follows [13]:

$$(\varepsilon_{BL} - \varepsilon_{AL})(\sigma_{BL} - \sigma_{AL}) = K_t^2(S_B - S_A)(e_B - e_A) \qquad d\overline{\varepsilon}_p < 0 \tag{7}$$

$$(\varepsilon_{CL} - \varepsilon_{BL})(\sigma_{CL} - \sigma_{BL}) = K_t^2(S_C - S_B)(e_C - e_B) \qquad d\overline{\varepsilon}_p \geq 0 \tag{8}$$

Subscript L represents the local stress and strain components at the notch root. Subscripts A, B, and C denote cyclic load turning points from zero to the maximum load (point A), the minimum load (point B), and the maximum load (point C). The stress concentration factor is defined as the ratio of the local stress to the applied stress. Backstress components for A, B, and C were then defined as $\alpha_{AL} = \frac{2}{3}(\sigma_{AL} - \sigma_y)$, $\alpha_{BL} = \frac{2}{3}(\sigma_{BL} + \sigma_y)$, and $\alpha_{CL} = \frac{2}{3}(\sigma_{CL} - \sigma_y)$ [39].

The Ramberg–Osgood [29] equation related the uniaxial nominal strain to the stress range as follows:

$$\Delta e = \frac{\Delta S}{E} + 2\left(\frac{\Delta S}{2K'}\right)^{\frac{1}{n'}} \tag{9}$$

To establish a connection between the nominal stress and the local strain, as well as the local stress, throughout the unloading and reloading paths of each stress cycle, Equations (7) and (8) were expressed as [13]:

$$(\varepsilon_B - \varepsilon_A)(\sigma_B - \sigma_A) = K_t^2(S_B - S_A)\left(\frac{S_B - S_A}{E} + 2\left(\frac{S_B - S_A}{2K'}\right)^{\frac{1}{n'}}\right) \quad d\bar{\varepsilon}_p < 0 \tag{10}$$

$$(\varepsilon_C - \varepsilon_B)(\sigma_C - \sigma_B) = K_t^2(S_C - S_B)\left(\frac{S_C - S_B}{E} + 2\left(\frac{S_C - S_B}{2K'}\right)^{\frac{1}{n'}}\right) \quad d\bar{\varepsilon}_p \geq 0 \tag{11}$$

where local stress and strain terms in Equations (7)–(11) are presented with Greek symbols. The terms n', K', and E correspond to the cyclic hardening exponent, the hardening coefficient, and materials elastic modulus, respectively.

3. Materials and Testing Conditions

A hot-rolled 1045 steel plate was cut to prepare cylindrical notched samples for tensile and cyclic tests [35–37]. Tensile properties of steel alloy were obtained under the monotonic loading and displacement-controlled conditions using a servo-hydraulic testing machine with a loading frequency between 25 and 30 Hz and a stress ratio of R = 0.9. Figure 1 presents samples tested under tensile and cyclic loading conditions. Samples in this figure consisted of semi-circular and V-shaped notches with stress concentration factors of K_t = 1.65 and 3.65, respectively. Test samples HT1–HT3 were heat-treated under different conditions as follows, respectively: at (i) 570 °C for two hours quenched to room temperature in air, resulting in a hardness of 12 RC; (ii) 870 °C for two hours, quenched in agitated oil for fifteen minutes at 74 °C, and tempered at 400 °C for two hours, producing 40 RC; and (iii) 870 °C for two hours, quenched in agitated oil for fifteen minutes at 74 °C and tempered at 315 °C for two hours, resulting in 50 RC. The modulus of elasticity and yield strength for samples HT1, HT2, and HT3 were (208 GPa, 490 MPa), (207 GPa, 1130 MPa), and (205 GPa, 1460 MPa), respectively [35–37]. For the heat-treated sample HT1, the prior austenitic grain size was between 6 and 7, characterized by a microstructure consisting of approximately 40% ferrite and 60% pearlite. For the HT2 sample, the microstructure predominantly comprised highly tempered martensite, with the prior austenitic grain size remaining at 7. Finally, in the third treated sample, HT3, the prior austenitic grain size ranged from 7 to 8. This treatment resulted in a microstructure primarily composed of approximately 75% tempered martensite, with fine pearlite. Figure 2 presents tensile stress–strain curves for notched 1045 as-received, HT1, HT2, and HT3 samples.

Uniaxial cyclic tests were conducted at different stress levels indexed by the ratio of maximum stress to ultimate strength for notched samples (S_{max}/S_{ult}) in percentage. The V-notched and semi-circular notched samples were tested under stress-controlled conditions and with a frequency of 25–30 Hz. Local strain data were measured at the notch root of samples through an extensometer displacement, as loading cycles were applied with a stress ratio of R = 0.9. Figure 3 plots ratcheting strains measured from the average of maximum and minimum local strains at the notch root for heat-treated 1045 steel samples at various stress levels S_{max}/S_{ult}. Different heat treatment conditions noticeably affected the ratcheting of notched samples. In Figure 3, for semi-circular and V-notched samples with a

stress concentration factor of $K_t = 1.65$ and 3.65, an increase in heat treatment temperature and tempering process in HT2 samples declined ratcheting at the notch root by as high as 65% as compared with HT1 samples. At a given applied stress level, V-shaped samples with K_t = 3.65 (see Figure 3b) were highly impacted as the tempering temperature for HT2 was adapted, while a semi-circular notch with K_t = 1.65 showed a slightly smaller drop in local ratcheting level in the HT2 sample as compared with the HT1 sample with no tempering process (see Figure 3a). Local ratcheting at the semi-circular notch in sample HT3 dropped as the magnitude of tempering temperature dropped from 400 °C to 315 °C.

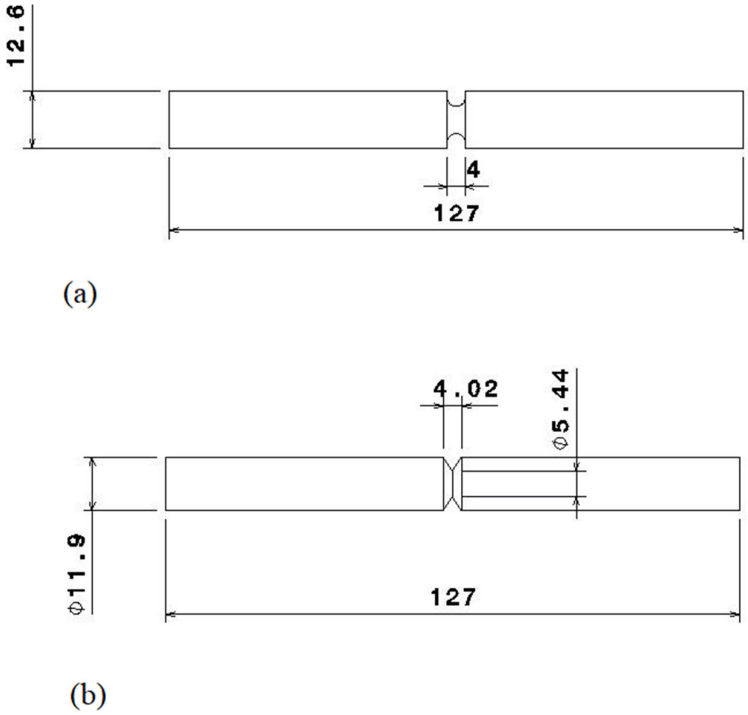


Figure 1. Samples' geometry: (**a**) $K_t = 1.65$, (**b**) $K_t = 3.65$ (all dimensions in mm).

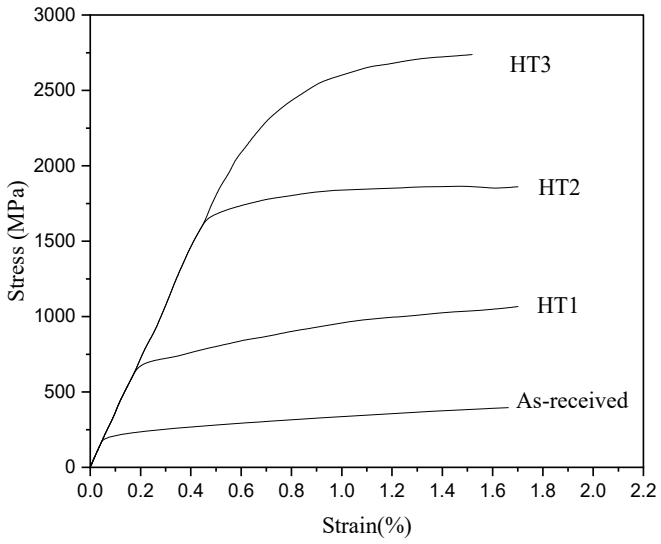


Figure 2. Monotonic stress–strain curves for as-received, HT1, HT2, and HT3 specimens.

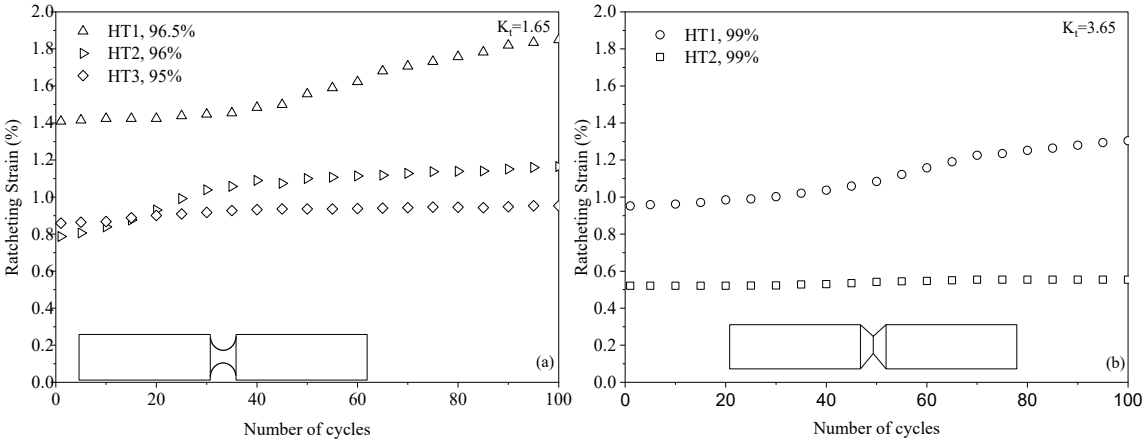


Figure 3. Ratcheting strain versus the number of cycles for notched 1045 steel samples tested at R = 0.9: (**a**) edge/semi-circular notch (K_t = 1.65), and (**b**) edge sharp notch (K_t = 3.65).

4. Finite Element Analysis

The finite element method (FEM) was employed to determine the Chaboche hardening model coefficients consistent with the hysteresis loop measured from the strain-controlled test. ABAQUS software version 6.13 containing the Chaboche materials model was used for this purpose [40]. The notched specimen was divided into quadratic elements for meshing, and constraints were applied to restrict the sample motion at one end. The upper surface of the specimen had translational and rotational axes restrained along the X and Z axes, while the specimen was allowed to carry the load along the Y axis. Uniaxial loading cycles were applied to the upper end of the specimen under stress-controlled conditions. Quadratic elements of type C3D8R were used with eight nodes per brick element, resulting in 3 degrees of freedom per node and a total of 24 degrees of freedom. The meshed samples around the notch are depicted in Figure 4.

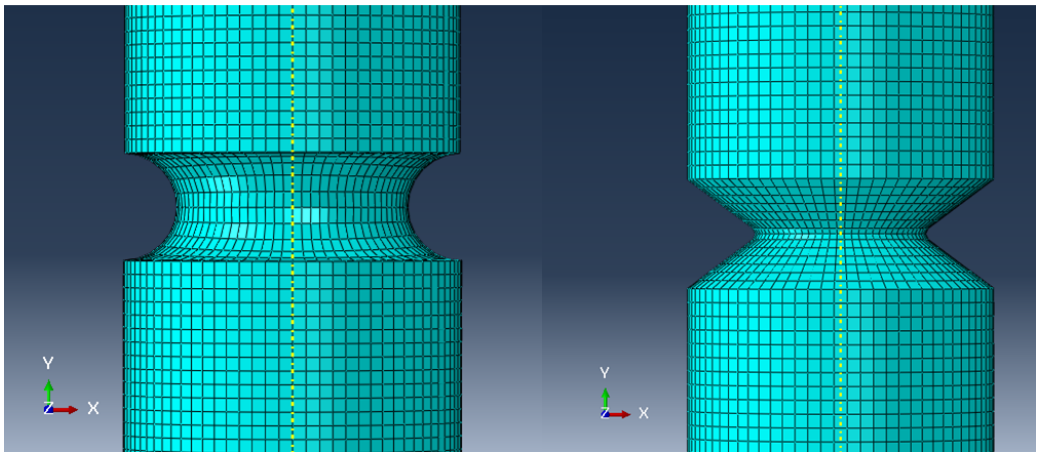


Figure 4. Meshed semi-circular and V-shaped notched samples.

5. Results and Discussion

The hardening frameworks of CH and A–V were employed along with the Neuber rule to assess the evolution of backstress and local ratcheting at the notch root of 1045 steel samples. The backstress increments and the yield surface translation were governed through the hardening frameworks. Different notch shapes, heat treatment post-processing conditions, and applied stress levels noticeably influenced the plastic strain progress at notch roots as samples experienced asymmetric loading cycles. To predict ratcheting at the notch root of heat-treated steel samples, we first defined terms and material coefficients in the hardening rules and then evaluated the backstress and yield surface evolution over the

loading excursion beyond the elastic limit. The predicted ratcheting values at the notch roots of steel samples were compared with those of measured values.

5.1. The A–V Hardening Rule Coefficients

Material coefficients C_1, γ_1, and γ_2 for 1045 steel samples were found to vary under different heat treatment conditions. Stress-controlled stress–strain hysteresis loops for HT1, HT2, and HT3 samples are presented in Figure 5. Figure 5a–d lists the values of coefficients C and γ_1 for as-received and heat-treated steel samples. The values of coefficient γ_2 were determined through the closest agreements of the predicted ratcheting curves with the measured values in Figure 5e.

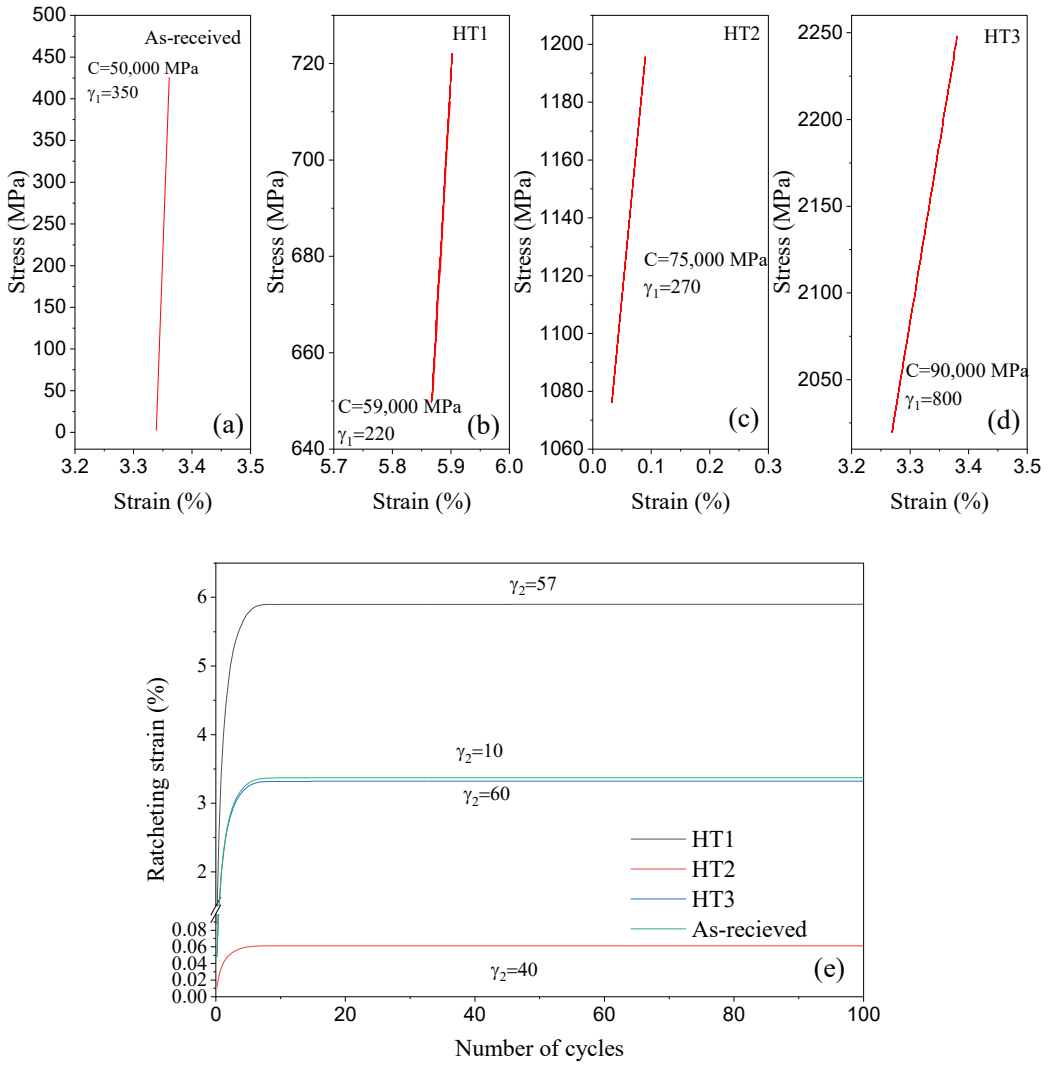


Figure 5. Coefficients of C, γ_1 for (**a**) as-received notched sample, (**b**–**d**) heat-treated HT1, HT2,HT3 notched 1045 steel samples, and (**e**) coefficient γ_2 for all notched samples.

5.2. The CH Hardening Rule Coefficients

The Chaboche hardening coefficients C_1, C_2, C_3, γ_1', γ_2', and γ_3' were determined through stress–strain hysteresis loops determined from the strain-controlled tests conducted in as-received and heat-treated steel samples at ±0.8% [41]. The values of these coefficients were determined to tightly agree between the predicted and experimental loops together through a number of trials. More details on how to determine these factors are described in an earlier published article [4]. Figure 6 plots the strain-based hysteresis loops predicted by the CH model versus the loops measured and reported in [41]. Coefficients C_{1-3} and γ_{1-3}' for the as-received and heat-treated 1045 steel samples are presented in Figure 6.

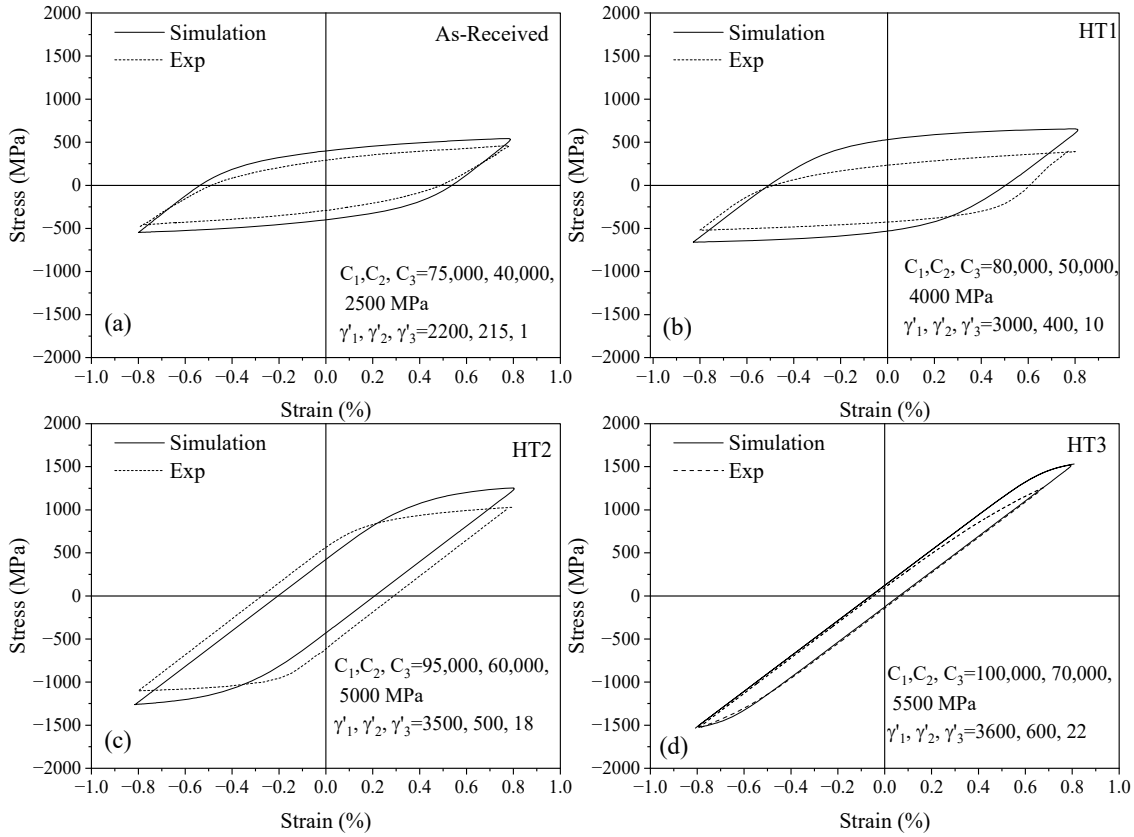


Figure 6. Strain-controlled hysteresis loops to determine coefficients C_{1-3} and γ'_{1-3} for heat-treated notched 1045 steel samples: (**a**) as-received sample, (**b**) heat-treated sample HT1, (**c**) heat-treated sample HT2, and (**d**) heat-treated sample HT3.

5.3. Backstress Increments and Yield Surface Translation

The onset of yielding demarcated the elastic and plastic domains through the von Mises yielding criterion, resulting in the formation of the yield surfaces presented in Figure 7. As the stress magnitude exceeded the materials yield limit, the yield surfaces were translated with an increase in the backstress increment through the kinematic hardening rule governance. The A–V model translated the yield surfaces in the deviatoric stress space and controlled the evolution and increment of the backstress term $(\overline{\alpha} - \delta\overline{b})$ through an internal variable $\overline{b}$. In Figure 7, the initial yield surfaces for the heat-treated samples of HT1, HT2, and HT3 are presented by solid elliptical surfaces in a $\sigma_1 - \sigma_2$ coordinate system. The initial yield surfaces for heat-treated samples intercepted the stress–strain curves at the yield points P_i, M_i, and N_i to signify the beginning of yielding. As materials at the notch root area exhibited a higher hardness and resistance against the yielding as a result of the heat treatment operations, the yield surfaces enlarged in stress and strain values, as in Figure 7a. The yield surface was largely translated into the deviatoric stress space by the A–V kinematic hardening rule intercepting the stress–strain curve at P_1, M_1, and N_1, as presented in Figure 7b. Heat-treated samples having a stress intensity factor of 1.65 with S_{max}/S_{ult} = 96.5%, 96%, and 95% for HT1, HT2, and HT3 were evaluated to observe the influence of the heat treatment process on materials yielding and strength.

The evolution of backstress throughout the loading cycles was controlled using the A–V and CH kinematic hardening procedures. The backstress increments and the internal variable $\overline{b}$ were regulated the through term $(\overline{\alpha} - \delta\overline{b})$ in the dynamic recovery term of the A–V model to achieve a steady state. The term $(\overline{\alpha} - \delta\overline{b})$ in the A–V model was found to be analogous to the Chaboche postulation integrating the backstress increments $d\overline{\alpha} = \sum_{i=1}^{3} d\overline{\alpha}_i$. In both the A–V and CH models, the evolution of backstress through the loading paths controlled the backstress increments and yield surface translation within the loading process

in the plastic domain. Figure 8 presents the evolution of backstress terms based on the A–V and CH models as loading cycles progressed. In this figure, a sudden drop in backstress over the first thirty cycles is evident. A steady condition was attained over the longer cycles, manifesting the higher dislocation interactions beyond the yielding point, lowering the ratcheting rate and leading to a steady state.

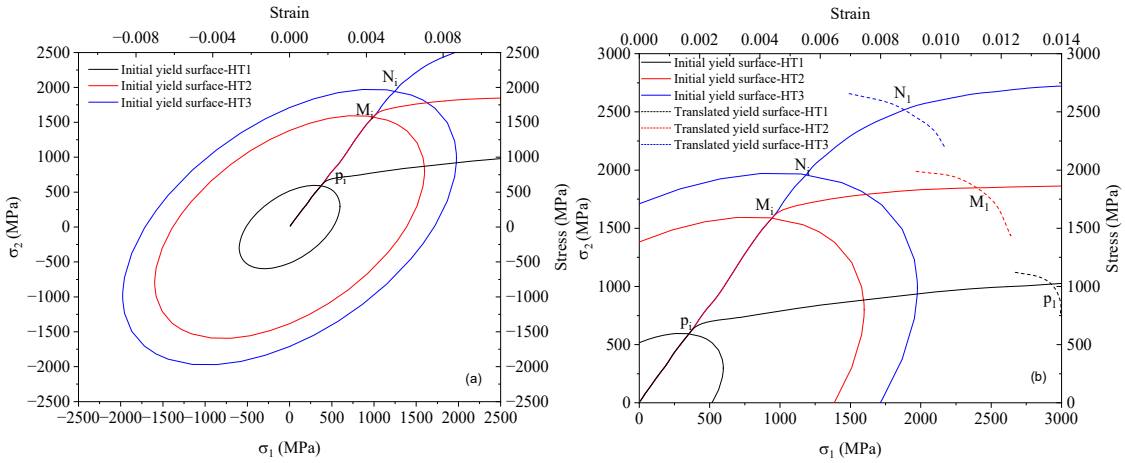


Figure 7. (**a**) Initial yield surfaces for heat-treated 1045 steel samples HT1, HT2, and HT3, and (**b**) translated yield surfaces for the heat-treated steel samples.

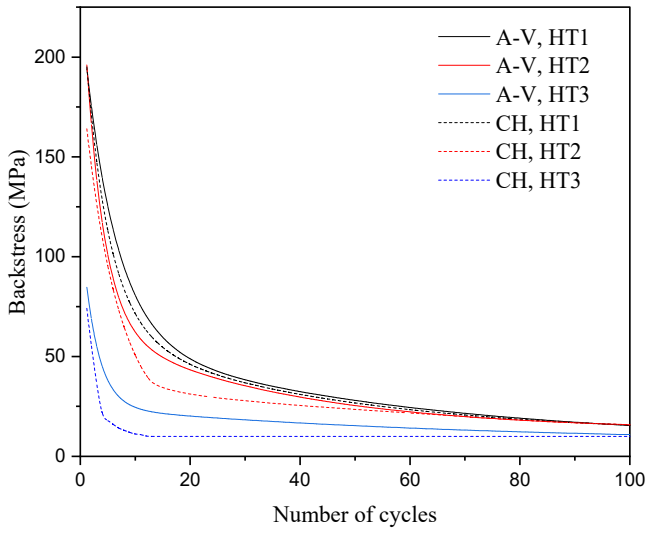


Figure 8. The evolution of the backstress term over the loading cycles based on the A–V model through term $(\overline{\alpha} - \delta\overline{b})$ and the Chaboche model through postulation $d\overline{\alpha} = \sum_{i=1}^{3} d\overline{\alpha}_i$.

5.4. Predicted Local Ratcheting

The A–V and CH kinematic hardening rules were coupled with Neuber's rule to assess the local ratcheting of heat-treated 1045 steel specimens subjected to asymmetric stress cycles. Figure 9 presents the local ratcheting of notched steel samples plotted versus asymmetric loading cycles. The predicted and measured ratcheting values of steel samples with semi-circular notches (K_t = 1.36) tested at stress ratios S_{max}/S_{ult} as high as 95–96% under different heat-treated conditions were presented in Figure 9a. Figure 9b presents ratcheting for samples with V-shaped notches (K_t = 3.65). The predicted and measured ratcheting results were found to be highly dependent on the notch shapes, the applied stress levels, and the heat treatment post-processing. The predicted ratcheting results were built up sharply over the first few cycles. The ratcheting rate declined as the number of cycles increased, resulting in mild progress. The heat treatment post-processing suppressed local

ratcheting as the notch root region possessed a high hardness and strength response. The local ratcheting progress for the steel sample HT1 with semi-circular notches ($K_t = 1.65$) heat treated at 570 °C for two hours and air-quenched and then tested at $S_{max}/S_{ult} = 0.965$ did not exceed 1.80% over the first one hundred loading cycles. This value decreased to 1.2% for the sample HT2, with an increase in the heat-treating temperature (870 °C) followed by tempering at 400 °C, and further dropped to 0.9% for the HT3 sample heat treated at 870 °C and tempered at 315 °C. Heat treatment post-processing affected the hardness and strength of materials within the notch root region and suppressed ratcheting at this region over the loading cycles. The decreasing trend in ratcheting strain with an increase in heat treatment temperature and tempering process in HT2 and HT3 samples was evident from predicted ratcheting curves based on the A–V and CH kinematic hardening rules. The A–V model slightly overestimated local ratcheting at the notch root, while the predicted curves through the CH model fell below the experimental data for different notch shapes and stress levels.

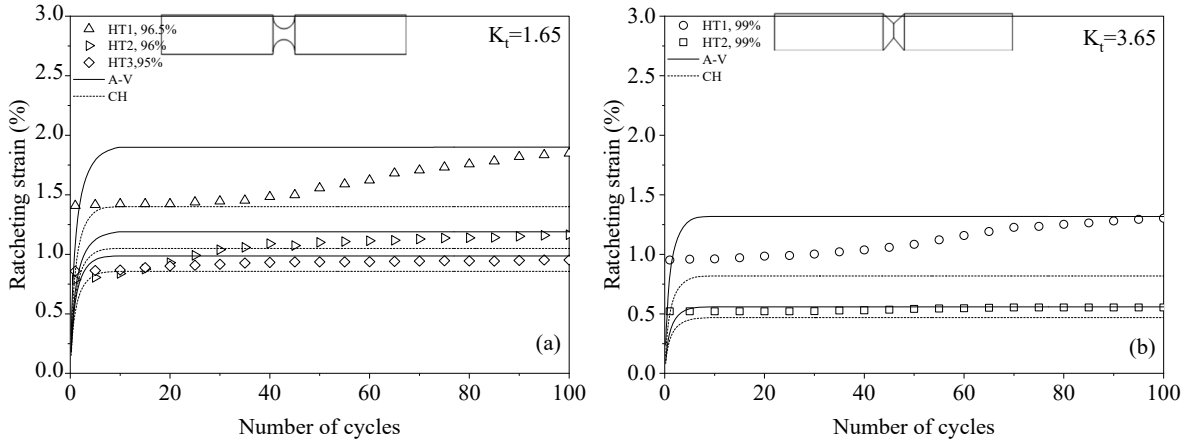


Figure 9. The measured ratcheting data and the predicted ratcheting curves based on the A–V and CH models for heat-treated 1045 steel samples with different notches of (**a**) semi-circular shapes (K_t = 1.65) and (**b**) V shapes (K_t = 3.65).

The local ratcheting response of 1045 steel notched samples was largely affected as samples were heat-treated under various conditions. The higher heat treatment temperature followed by the tempering process relieved some residual stresses at the notch region and improved materials hardness and strength. The hardened notch region resisted the ratcheting deformation in samples HT2 and HT3 as compared with sample HT1, with the lower heat treatment temperature and no tempering process. The A–V and CH hardening frameworks have resulted in a gradual decline in backstress over the loading process within the plastic domain. The hardening rules along with Neuber's rule enabled a consistent local ratcheting assessment under different stress levels and notch shapes. The backstress evolution based on the A–V model showed a gradual drop over the loading cycles to steady condition in an analogous trend as the CH postulation offered. While the parameters including the applied stress level, cyclic stress ratio, notch size and shape, and heat treatment post-processing are crucial technical variables in the local ratcheting response of materials, the choice of hardening rule, notch root analysis model, and hardening coefficients and materials constants are prime analytical and computational ingredients in ratcheting evaluation at the notch root of samples. The authors believe that heat treatment and other post-processing treatments including press fitting and cold expansion largely influence the ratcheting magnitude and rate at the materials surrounding the notch root. More research is demanded to accurately evaluate the influence of technical and analytical parameters on ratcheting assessment at notch roots. The next immediate research plan is set to further evaluate the ratcheting of materials at the notch root region, where materials are pre-strained through a cold rolling process.

6. Conclusions

The local ratcheting response of heat-treated 1045 steel samples with notch shapes under asymmetric loading cycles was investigated. The ratcheting assessment was conducted through the use of the hardening frameworks structured based on the A–V and CH kinematic hardening rules in conjunction with the Neuber rule. Hardening coefficients were affected by heat treatment post-processing. The higher heat treatment temperature and tempering process in samples TH2 and TH3 resulted in the alleviation of the residual stress at the notch root of steel samples, suppressing the ratcheting progress in these samples. Hardening frameworks governed the incremental backstress progress and their related yield surface translations in the deviatoric stress space for loads beyond the elastic limit. Heat treatment post-processing highly influenced the backstress evolution and yield surfaces over the loading process. The choice of heat treatment process enhanced the materials strength and hardness and controlled the progression of ratcheting at the notch roots over the loading process.

Author Contributions: Conceptualization, F.H. and A.V.-F.; methodology, A.V.-F.; software, A.V.-F.; validation, F.H. and A.V.-F.; formal analysis, F.H. and A.V.-F.; investigation, F.H. and A.V.-F.; data curation, A.V.-F.; writing—original draft preparation, F.H.; writing—review and editing, A.V.-F.: visualization, F.H.; supervision, A.V.-F.; project administration, A.V.-F.; funding acquisition, A.V.-F.; All authors have read and agreed to the published version of the manuscript.

Funding: This research was funded by the Natural Sciences and Engineering Research Council of Canada (NSERC) through A.V.-F., grant number RGPIN-2021-03047.

Institutional Review Board Statement: Not applicable.

Informed Consent Statement: Not applicable.

Data Availability Statement: The data presented in this study are openly available reference numbers [35–37].

Conflicts of Interest: The authors declare no conflicts of interest.

Nomenclature

$d\bar{\varepsilon}$	Total strain increment tensor
$d\bar{\varepsilon}_e$	Elastic strain increment tensor
$d\bar{\varepsilon}_p$	Plastic strain increment tensor
E	Modulus of elasticity
H_p	Plastic modulus
$\bar{\alpha}$	Backstress tensor
$\bar{\sigma}$	Stress tensor
$\bar{I}$	Unit tensor
ϑ	Poisson's ratio
G	Shear modulus
$\bar{s}$	Deviatoric stress tensor
σ_y	Yield strength
D	Circular notch diameter
$\gamma_1, \gamma_2, C, \delta$	Coefficients of the A-V model
C_{1-3}, γ'_{1-3}	Chaboche materials coefficients
K_t	Stress concentration factor
$\bar{b}$	Internal variable of the A-V model tensor
n', K'	Ramberg-Osgood coefficients
S, e	Nominal stress and strain
R	Stress ratio
K_σ, K_ε	Stress and strain concentration factors
σ, ε	Uniaxial local stress and strain at the notch root

References

1. Wang, C.H.; Rose, L.R.F. Transient and steady-state deformation at notch root under cyclic loading. *Mech. Mater.* **1998**, *30*, 229–241. [CrossRef]
2. Hu, W.; Wang, C.H.; Barter, S. *Analysis of Cyclic Mean Stress Relaxation and Strain Ratchetting Behavior of Aluminum 7050*; Aeronautical and Maritime Research Lab Melbourne (Australia): Melbourne, Australia, 1999.
3. Rahman, S.M.; Hassan, T. Advanced cyclic plasticity models in simulating ratcheting responses of straight and elbow piping components, and notched plates. In Proceedings of the ASME Pressure Vessels and Piping Conference, Denver, CO, USA, 17–21 July 2005; pp. 421–427.
4. Chaboche, J. On some modifications of kinematic hardening to improve the description of ratcheting effects. *Int. J. Plast.* **1991**, *7*, 661–678. [CrossRef]
5. Ohno, N.; Wang, J.D. Kinematic hardening rules with critical state of dynamic recovery, part I: Formulations and basic features for ratcheting behavior. *Int. J. Plast.* **1993**, *9*, 375–390. [CrossRef]
6. Ohno, N.; Abdel Karim, M. Uniaxial ratcheting of 316FR steel at room temperature—Part II: Constitutive modeling and simulation. ASME J. *Appl. Mech.* **2000**, *122*, 35–41.
7. Firat, M. A notch strain calculation of a notched specimen under axial-torsion loadings. *Mater. Des.* **2011**, *32*, 3876–3882. [CrossRef]
8. Neuber, H. Theory of stress concentration for shear-strained prismatical bodies with arbitrary nonlinear stress-strain law. *J. Appl. Mech.* **1961**, *28*, 544–550. [CrossRef]
9. Barkey, M.E. Calculation of Notch Strains under Multiaxial Nominal Loading. Ph.D. Thesis, Department of Theoretical and Applied Mechanics, University of Illinois at Urbana-Champaign, Illinois City, IL, USA, 1993.
10. Liu, C.; Shi, S.; Cai, Y.; Chen, X. Ratcheting behavior of pressurized-bending elbow pipe after thermal aging. *Int. J. Press. Vessel. Pip.* **2019**, *169*, 160–169. [CrossRef]
11. Chen, X.; Jiao, R.; Kim, K.S. On the Ohno-Wang kinematic hardening rules for multiaxial ratcheting modeling of medium carbon steel. *Int. J. Plast.* **2005**, *21*, 161–184. [CrossRef]
12. Kolasangiani, K.; Farhangdoost, K.; Shariati, M.; Varvani-Farahani, A. Ratcheting assessment of notched steel samples subjected to asymmetric loading cycles through coupled kinematic hardening-Neuber rules. *Int. J. Mech. Sci.* **2018**, *144*, 24–32. [CrossRef]
13. Shekarian, A.; Varvani-Farahani, A. Ratcheting prediction at the notch root of steel samples over asymmetric loading cycles. *J. Eng. Mater. Technol. Trans.* **2020**, *142*, 1–23. [CrossRef]
14. Shekarian, A.; Varvani-Farahani, A. Concurrent ratcheting and stress relaxation at the notch root of steel samples undergoing asymmetric tensile loading cycles. *Fatigue Fract. Eng. Mater. Struct.* **2019**, *42*, 1402–1413. [CrossRef]
15. Shekarian, A.; Varvani-Farahani, A. Ratcheting behavior of notched stainless-steel samples subjected to asymmetric loading cycles. *J. Iron Steel Res. Int.* **2021**, *28*, 86–97. [CrossRef]
16. Shekarian, A.; Varvani-Farahani, A. Ratcheting response of SS316 steel samples with different notch shapes under various loading spectra. *J. Mater. Eng. Perform.* **2021**, *30*, 3524–3535. [CrossRef]
17. Armstrong, P.J.; Frederick, C.O. *A Mathematical Representation of the Multiaxial Bauschinger Effect, CEGB Rep. RD/B/N, 731*; Berkeley Nuclear Laboratories: Berkeley, CA, USA, 1966.
18. Ahmadzadeh, G.R.; Varvani-Farahani, A. Ratcheting assessment of materials based on the modified Armstrong–Frederick hardening rule at various uniaxial stress levels. *Fatigue Fract. Eng. Mater. Struct.* **2013**, *36*, 1232–1245. [CrossRef]
19. Hatami, F.; Varvani-Farahani, A. Accumulation of plastic strain at notch root of steel specimens undergoing asymmetric fatigue cycles: Analysis and simulation. *Materials* **2023**, *16*, 2153. [CrossRef] [PubMed]
20. Weiyuan, N.; Shanglei, Y.; Jin, J.; Jianying, B.; Yangshenglan, L. Fatigue property of Al-5Zn-2Mg aluminum alloy welding joints used in high-speed trains. *Rare Met. Mater. Eng.* **2016**, *45*, 2774–2778. [CrossRef]
21. Duan, C.; Yang, S.; Gu, J.; Xiong, Q.; Wang, Y. Microstructure and ratcheting behavior of 6061 aluminum alloy laser-MIG hybrid welding joint. *Mater. Res. Express* **2019**, *6*, 086534. [CrossRef]
22. Wang, H.; Jing, H.; Zhao, L.; Han, Y.; Lv, X.; Xu, L. Uniaxial ratcheting behaviour of 304L stainless steel and ER308L weld joints. *Mater. Sci. Eng.* **2017**, *708*, 21–42. [CrossRef]
23. Gioielli, P.; Buitrago, J.; Kan, W.; Weir, M.; Chell, G.; Hudak, S.J., Jr. Calibration of Flaw Extension Model Under Ratcheting Fatigue. In Proceedings of the International Conference on Offshore Mechanics and Arctic Engineering, Honolulu, HW, USA, 31 May–5 June 2009; pp. 267–277.
24. Schmiedt, A.; Manka, M.; Tillmann, W.; Walther, F. Local quasi-static and cyclic deformation behaviour of brazed AISI 304L/BAu-4 joints characterised by digital image correlation. *Weld. World* **2019**, *63*, 501–509. [CrossRef]
25. Chakherlou, T.N.; Vogwell, J. A novel method of cold expansion which creates near-uniform compressive tangential residual stress around a fastener hole. *Fatigue Fract. Eng. Mater. Struct.* **2004**, *27*, 343–351. [CrossRef]
26. Chakherlou, T.N.; Aghdam, A.B. An experimental investigation on the effect of short time exposure to elevated temperature on fatigue life of cold expanded fastener holes. *Mater. Design* **2008**, *29*, 1504–1511. [CrossRef]
27. Chakherlou, T.N.; Mirzajanzadeh, M.; Saeedi, K.H. Fatigue crack growth and life prediction of a single interference fitted holed plate. *Fatigue Fract. Eng. Mater. Struct* **2010**, *33*, 633–644. [CrossRef]
28. Chakherlou, T.N.; AJRI, M. Strain ratcheting and stress relaxation around interference-fitted single-holed plates under cyclic loading: Experimental and numerical investigations. *Fatigue Fract. Engng. Mater. Struct.* **2012**, *36*, 327–339. [CrossRef]

29. Tripathy, S.; Mondal, A.K.; Dutta, K. Effect of pre-strain on ratcheting behavior of A668 Class D steel. In Proceedings of the IOP Conference Series: Materials Science and Engineering, Rourkela, India, 12–13 December 2016; p. 012037.
30. Hatami, F.; Varvani-Farahani, A. Local Ratcheting at the Notch Region of Non-Press-Fitted and Press-Fitted Al 7075-T6 Samples Undergoing Asymmetric Stress Cycles. *Metals* **2023**, *13*, 1549. [CrossRef]
31. Kreethi, R.; Verma, P.; Dutta, K. Influence of heat treatment on ratcheting fatigue behavior and post ratcheting tensile properties of commercial aluminum. *Trans. Indian Inst. Met.* **2015**, *68*, 229–237. [CrossRef]
32. Kreethi, R.; Mondal, A.K.; Dutta, K. Ratcheting fatigue behaviour of 42CrMo4 steel under different heat treatment conditions. *Mater. Sci. Eng.* **2017**, *A 679*, 66–74. [CrossRef]
33. Azadi, M.; Basiri, A.; Dadashi, A.; Winter, G.; Seisenbacher, B.; Gruen, F. Effect of nano-clay addition and heat-treatment on tensile and stress-controlled low-cycle fatigue behaviors of aluminum-silicon alloy: Effect of nano-clay addition and heat-treatment. *Frat. Ed Integrità Strutt.* **2021**, *15*, 373–397. [CrossRef]
34. Xu, X.; Wang, Z.; Gao, G.; Zhang, X.; Kang, G.; Kan, Q. The effect of microstructure evolution on the ratchetting-fatigue interaction of carbide-free bainite rail steels under different heat-treatment conditions. *Int. J. Fatigue* **2022**, *160*, 106872. [CrossRef]
35. Pals, T.G.; Stephens, R.I. The influence of high R ratio on mild and sharp notched and unnotched fatigue behavior of 1045 steel with three different heat treatments. *Int. J. Fatigue* **2004**, *26*, 651–661. [CrossRef]
36. Karadag, M.; Stephens, R.I. The influence of high R ratio on unnotched fatigue behavior of 1045 steel with three different heat treatments. *Int. J. Fatigue* **2003**, *25*, 191–200. [CrossRef]
37. Vantiger, T.R.; Stephens, R.I.; Karadag, M. The influence of high R ratio on notched fatigue behaviour of 1045 steel with three different heat treatments. *Int. J. Fatigue* **2002**, *24*, 1275–1284. [CrossRef]
38. Varvani-Farahani, A. A comparative study in descriptions of coupled kinematic hardening rules and ratcheting assessment over asymmetric stress cycles. *Fatigue Fract. Eng. Mater. Struct.* **2017**, *40*, 882–893. [CrossRef]
39. Rezaiee-Pajand, M.; Sinaie, S. On the calibration of the Chaboche hardening model and a modified hardening rule for uniaxial ratcheting prediction. *Int. J. Solids Struct.* **2009**, *46*, 3009–3017. [CrossRef]
40. Abaqus Inc. *ABAQUS User's Manual. Version 6.13*; Hibbitt, Karlsson & Sorensen, Incorporated: Pennsylvania, LA, USA, 2016.
41. Kolasangiani, K. Analysis of Local and Global Ratcheting Behavior of AISI 1045 Steel Specimens with Cutout. Ph.D. Thesis, Department of Mechanical Engineering, Ferdowsi University of Mashhad, Razavi Khorasan, Iran, 2018.

Disclaimer/Publisher's Note: The statements, opinions and data contained in all publications are solely those of the individual author(s) and contributor(s) and not of MDPI and/or the editor(s). MDPI and/or the editor(s) disclaim responsibility for any injury to people or property resulting from any ideas, methods, instructions or products referred to in the content.